

# Climate change impact on future photovoltaic resource potential in an orographically complex archipelago, the Canary Islands

Juan C. Pérez <sup>a,\*</sup>, Albano González <sup>a</sup>, Juan P. Díaz <sup>a</sup>, Francisco J. Expósito <sup>a</sup>, Jonatan Felipe <sup>b</sup>

<sup>a</sup> Grupo de Observación de la Tierra y la Atmósfera (GOTA), Universidad de La Laguna (ULL), Canary Islands, Spain

<sup>b</sup> Área de Tecnología, Instituto Tecnológico y de Energías Renovables (ITER), Canary Islands, Spain

## ARTICLE INFO

### Article history:

Received 29 June 2018

Received in revised form

12 October 2018

Accepted 16 October 2018

Available online 20 October 2018

### Keywords:

photovoltaic power

Climate change

Energy projections

The Canary islands

## ABSTRACT

It is widely accepted by the scientific community that in the coming decades the Earth's climate will undergo significant changes, which will affect the ecosystems and the population in various ways. In this work, climate change impacts on solar photovoltaic (PV) resources were evaluated in the Canary Islands, an orographically complex archipelago located in the sub-tropical Atlantic Ocean, using high resolution dynamical downscaling techniques. To alleviate the high computational cost of high resolution simulations, the pseudo-global warming technique was used to compute the initial and boundary conditions from a reanalysis dataset and from the monthly mean changes obtained by the simulations of fourteen global climate models included in the Coupled Model Intercomparison Project Phase 5 (CMIP5). Projections of annual-mean daily irradiation and PV potential were obtained for two future decades (2045–2054 and 2090–2099) and for two different greenhouse gas emission scenarios (RCP4.5 and RCP8.5), and the corresponding results were compared with those for a recent period (1995–2004). During winter, a generalized increase in PV potential is expected, as a consequence of a reduction in cloud cover. However, during summer, future simulations indicate a decrease in PV potential because of the rise of temperature and, therefore, a reduction in PV panel efficiency.

© 2018 Elsevier Ltd. All rights reserved.

## 1. Introduction

Greenhouse gas (GHG) emissions, associated with energy generation services, are a major cause of climate change [1]. There are several options for lowering GHG emissions while still satisfying the human demand for energy services. In this context, renewable energy sources play an important role in providing these services in a sustainable manner, contributing in this way to climate change mitigation [2]. Nevertheless, in turn, changes in renewable energy resources are expected as a consequence of climate warming. So, when considering the installation of a renewable energy power plant, it is important not only to assess the present renewable resources but also their possible changes in the future, especially if long-term operation and investment are planned [3]. In general, climate change projections are necessary for long-term energy and adaptation policies and greenhouse gas abatement strategy development [4–6].

In the case of solar energy, changes in cloud cover, which

directly affects the surface downwelling shortwave radiation, is the most important climate factor to be taken into account. Some authors suggest the planning of possible (re)location of PV plants based on expected changes in cloud cover [7]. To a lesser extent, both wind speed and temperature also affect the production of electricity by photovoltaic systems, as they modify their environmental conditions and, therefore, their efficiency [8,9]. Furthermore, the aerosol content of the atmosphere also modifies the solar radiation due to two different processes, their direct interaction through scattering and absorption, and their capacity to modify the microphysical properties of clouds, acting as cloud condensation nuclei, known as indirect effect.

The future assessment of energy resources is crucial for fragmented territories, such as archipelagos, where power grids are isolated preventing exchange of energy with other balancing areas. This is the case of the Canary Islands, a Spanish archipelago located to the northwestern of the African coast, centered approximately at 28° N, 16° W. The electricity system of the Canary Islands is broken down into six electrically isolated subsystems, one per island (Tenerife, Gran Canaria, La Palma, La Gomera and El Hierro) and another one for Lanzarote and Fuerteventura, whose grids are

\* Corresponding author.

E-mail address: [jcperez@ull.es](mailto:jcperez@ull.es) (J.C. Pérez).

joined by a submarine cable. The Archipelago, due to its climate characteristics and its latitude, has an abundant supply of renewable energy resources, mainly from the sun and wind. At the end of 2016, renewable power accounted for 12% (355 MW) of the total installed power capacity in the islands, of which 166 MW was solar photovoltaic [10]. The total energy demand in the Canary Islands presents an annual cycle, with a higher power consumption during summer and at the beginning of autumn and with lower demand during spring. In Fig. 1 the annual cycle for the last four years is plotted, based on the data provided by the transmission agent and operator of the Spanish electricity system [11]. The monthly photovoltaic and wind energy production are also shown. As expected, the highest photovoltaic production corresponds to summer, when the solar radiation is at its maximum. The annual cycle of the wind energy production peaks during summer, when the trade winds are stronger and more persistent. During this season, the wind energy production is twice the photovoltaic production.

Long-term changes in solar radiation, and the other mentioned climate variables, have been studied using global climate models (GCMs). Some authors [12,13], for example, used projections from different climate models from the Coupled Model Intercomparison Project Phases 3 (CMIP3) and 5 (CMIP5) to study the influence of expected changes in solar radiation on photovoltaic production worldwide. Another study [14] analyzed the impact of climate change on solar resources in a particular region, southern Africa, using GCMs from CMIP3. However, the spatial resolution of GCMs is too coarse for regional climate studies, because they cannot resolve local atmospheric phenomena or represent the topography in an adequate way, especially in orographically complex areas. To overcome these limitations, regional climate models (RCMs) are required [15]. During the recent decades, as a consequence of the increase in computer power, statistical and dynamical downscaling methods have been developed in order to improve the projections climate simulations provided by GCMs at a regional scale. Thus, some authors have used RCMs to estimate climate change effects on photovoltaic production in Europe [16] or in particular countries [17,18].

In this work, dynamical climate regionalization is used to estimate future changes in solar radiation, temperature and wind speed, and their effects on the photovoltaic potential, in the Canarian Archipelago, in the middle and at the end of this century. The Weather Research and Forecasting (WRF) model [19] was selected as the regional climate model (RCM). Unlike previous similar studies, which were based on larger regions, this work is focused on an archipelago composed of small islands with a very complex orography, which requires a high spatial resolution, in this case 5 km, to account for all the atmospheric phenomena that occur at

those scales. In this region, clouds do not only develop in small regions, but they are also blocked by the high mountains. All these circumstances complicate the computation of the mentioned variables, needed to estimate the photovoltaic potential. To alleviate the high computational cost associated with the high spatial resolution and the long simulation periods, the pseudo-global warming (PGW) method [20–22] has been used to obtain the regionalized climatology for the Canary Islands. Due to the great spatial variability of the irradiance in the study area, both data from ground instruments and two observational databases, based on satellite data and with a spatial resolution similar to WRF simulations, were used to assess simulated results for the historical period.

The outline of this article is as follows. The configuration of WRF to simulate the variables of interest for present and future periods is described in Section 2. In this section, the observational data used to compare WRF simulation results, and the definition of the computed variables, such as the PV potential, are also explained. In Section 3 the results for both, present period simulation assessment and future projections, are presented. Finally, the conclusions are summarised in the last section.

## 2. Methodology and data

In this section the configuration of the WRF model and the computation of the initial and boundary conditions from the reanalysis data and from the results of the CMIP5 global climate models are explained. The observational data used to validate WRF results and the method to compute monthly mean solar irradiation from sunshine duration are also presented. Finally, the models used to calculate PV potential from the solar irradiation, air temperature and wind speed are outlined.

### 2.1. Model setup

In this study, WRF, version 3.4.1, was used to perform the downscaling simulations. Three domains (Fig. 2), in a double-nested configuration, were defined, which correspond to spatial resolutions of 45, 15, and 5 km, respectively. All of these domains have been discretized with 32 vertical eta levels. The choice of the particular physical parameterizations, used to represent the different sub-grid scale atmospheric processes, and the version of the WRF model was done according to previous studies in the same area [23,24]. Thus, radiation schemes were set to the Community Atmosphere Model, version 3 (CAM3) for both longwave and shortwave [25,26]. In the domains with horizontal resolutions over 10 km, D1 and D2, where the fluxes cannot be explicitly resolved, Kain-Fritsch cumulus parameterization [27] was used, and no cumulus parameterization was applied in the innermost domain, D3. The planetary boundary layer was characterized using the Yonsei University scheme [28] and the land surface scheme was the Noah model [29]. Finally, the WRF double-moment 6-class (WDM6) [30] was used as the cloud microphysics scheme.

The shortwave scheme plays an important role in the computation of irradiance. The CAM3 shortwave solar radiation scheme is part of the Community Atmosphere Model. It considers gaseous absorption by ozone, carbon dioxide, oxygen and water vapor. Molecular scattering and scattering/absorption by cloud droplets and aerosols are also considered. The solar spectrum is divided into 19 discrete spectral and pseudo-spectral intervals. Layer reflections and transmissions are computed using the  $\delta$ -Eddington approximation. Five chemical species of aerosol are used in this parameterization, including sea salt, soil dust, black and organic carbonaceous aerosols, sulfate, and volcanic sulfuric acid. They are characterized by their specific extinction, single scattering albedo,

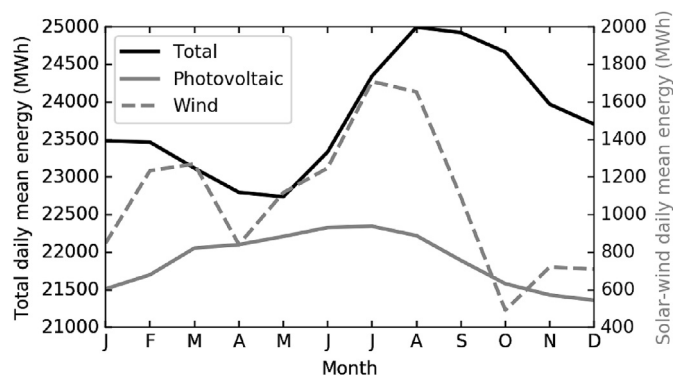
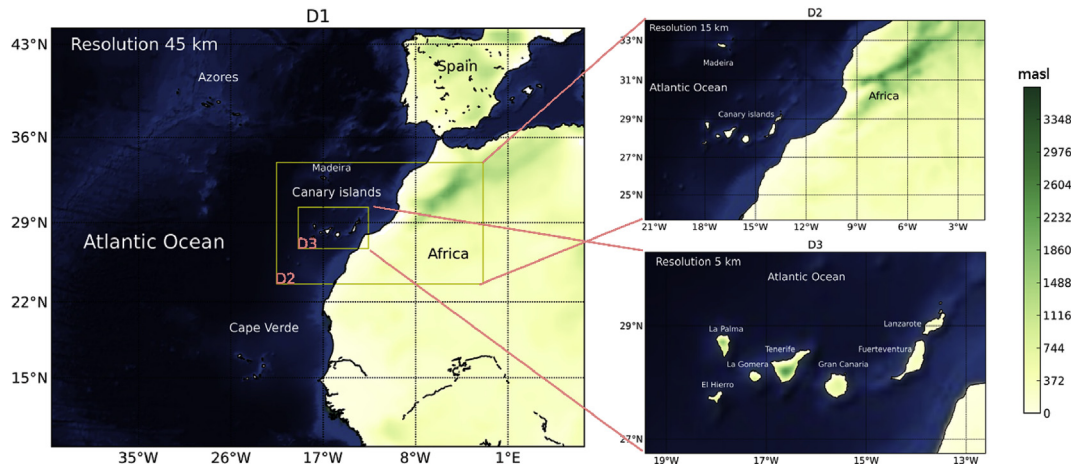


Fig. 1. Total energy demand and photovoltaic and wind energy production in the Canary Islands, expressed as daily mean values, for the period 2014–2017.



**Fig. 2.** Domains used in the WRF simulations. The coarse domain (D1) has a horizontal resolution of 45 km, D2 of 15-km, and the innermost domain (D3) a resolution of 5 km. Land surface height (m asl) is indicated in the color palette to highlight the complex orography of the studied region. (For interpretation of the references to color in this figure legend, the reader is referred to the Web version of this article.)

and asymmetry parameter. The ability of WRF simulations, using this scheme, to compute surface irradiances has been studied in some works [31,32], finding that CAM3 is one of the best options of the shortwave radiation schemes available in WRF.

The PGW approximation was used for climate regionalization following the same configuration used in previous studies [33,34], in which future changes in temperature, precipitation and wind were analysed. The climatology for a recent period (1995–2004) was obtained through WRF simulation, using ERA-Interim reanalysis data [35] as initial and boundary conditions. The use of reanalysis data, and not from a GCM, constitutes one of the main advantages of PGW methodology, because biases in the boundary conditions, in respect to the real climatology, are much lower [20]. For future periods, 2045–2054 and 2090–2099, initial and boundary conditions for the WRF integrations are given by the sum of a climate perturbation signal to the same ERA-Interim data used for the recent period simulation. This perturbation signal was computed, for those variables used as boundary conditions, from the results of 14 CMIP5-GCM (Table 1) projections, averaging their monthly mean values [33]. For each future period two different greenhouse gas concentration pathways, the CMIP5 RCP4.5 and RCP8.5 scenarios [36] were used, representing scenarios of medium

and high emission assumptions, respectively. They use emission pathways which lead to radiative forcings of 4.5 and 8.5  $\text{Wm}^{-2}$  at the end of this century, that correspond to greenhouse gas concentrations of approximately 650 and 1370 ppm  $\text{CO}_2$  equivalent [37]. For each experiment the model was integrated for an eleven-year period, taking the first year as spin-up, and it was not considered in any further analysis.

Usually, climate simulations comprise of larger periods, approximately thirty years as used for observations [38], however the PWG method allows us to use shorter simulation periods [39,40], which is another of the advantages of this methodology. This is particularly important for those regions that, due to their topography, require high resolution simulations and, therefore, high computational efforts. Despite the above mentioned advantages of PGW, this approximation also has some limitations. For example, it cannot adequately capture potential changes in the variability from daily to interannual time scales, because it assumes unchanged variability in the future climate. Furthermore, it assumes that frequency and intensity of weather perturbations that enter the regional simulation domain remains also unchanged, because they depend on the reanalysis data. These drawbacks make this method inadequate for studying future changes in extreme

**Table 1**

CMIP5 models used in this work to obtain the ensemble of perturbation signal for the PGW method. More information about models and the main references for each of them can be found in Ref. [1].

Model	Institution(s)	Country
ACCESS1.3	Commonwealth Scientific and Industrial Research Organization (CSIRO) and Bureau of Meteorology (BOM)	Australia
BCC-CSM1.1	Beijing Climate Center, China Meteorological Administration	China
CanESM2	Canadian Center for Climate Modelling and Analysis	Canada
CCSM4	US National Centre for Atmospheric Research	United States
CSIRO-Mk3.6.0	Queensland Climate Change Centre of Excellence and Commonwealth Scientific and Industrial Research Organisation	Australia
EC-EARTH	Europe	Europe
GFDL-ESM2G	NOAA Geophysical Fluid Dynamics Laboratory	United States
HadGEM2-ES	UK Met Office Hadley Centre	United Kingdom
INM-CM4	Russian Institute for Numerical Mathematics	Russia
IPSL-CM5A-MR	Institut Pierre Simon Laplace	France
MIROC5	University of Tokyo, National Institute for Environmental Studies, and Japan Agency for Marine-Earth Science and Technology	Japan
MPI-ESM-MR	Max Planck Institute for Meteorology	Germany
MRI-ESM1	Meteorological Research Institute	Japan
NorESM1-M	Norwegian Climate Centre	Norway

events, such as severe storms, strong winds, etc. Nevertheless, the consideration of these events is not essential to compute photovoltaic production, even though they could damage the solar panels.

## 2.2. Photovoltaic power potential

The energy produced by a PV array can be modeled as a function of the nominal power of the particular array, its response to the temperature, the incident solar irradiance, the air temperature and the wind speed [8]. Following that work, the photovoltaic power produced by an array ( $P_m$ ) can be expressed by:

$$P_m(t) = P_p \cdot \eta(t) \cdot \frac{G(t)}{G_{STC}} = P_p \cdot PVpot(t), \quad (1)$$

where  $P_p$  is the nominal power of the PV array under study, which is given by the manufacturer at standard test conditions (STC),  $G(t)$  is the solar irradiance, that is, the surface-downwelling shortwave radiation,  $G_{STC}$  corresponds to the solar irradiance at STC,  $1000 \text{ W m}^{-2}$ , and  $\eta(t)$  is a coefficient that includes all factors that are related with the actual energy produced by the PV array with the energy that would be produced if it were operating at STC. At the right hand of the equation, all the terms that depend on the solar radiation and atmospheric conditions have been grouped in a new term, PV potential (PVpot). PVpot allows characterizing a site, regardless of the nominal power of the PV array located on it. PVpot is a dimensionless variable that equals 1 when the ambient conditions are considered as STC, and it will be lower (higher) than the unit when the ambient conditions allow PV power output to be lower (higher) than the nominal power of the considered PV array. As proposed in a previous study [16], PVpot will be used to study the effects of climate change on the PV resources. The coefficient  $\eta$  must take into account those factors that represent the deviation of the real conditions in which the PV module is operating with respect to that specified as STC. These factors are, among others, the difference between the operating PV cell temperature and the standard ( $25^\circ\text{C}$ ), the cleanness of the PV module surface, the aging of the module or losses in the conductors. In this work, we consider that all these factors remain constant and, then, they do not contribute to changes in PVpot, except the PV cell temperature. So, PV module performance ratio can be expressed as [8]:

$$\eta_T(t) = 1 + \gamma(T_{cell}(t) - T_{STC}), \quad (2)$$

where  $\gamma$  is the maximum power thermal coefficient,  $T_{cell}$  the operation cell temperature and  $T_{STC}$  the cell temperature at STC ( $25^\circ\text{C}$ ). The  $\gamma$  coefficient is taken as  $-0.005^\circ\text{C}^{-1}$ , which corresponds to a monocrystalline silicon solar panel. In this way, the efficiency of the panel diminishes as the temperature is higher than  $T_{STC}$ . The cell temperature must be parameterized as a function of other variables that can be obtained from WRF simulations. In a previous study [9], different approximations to obtain  $T_{cell}$  from incident solar irradiance, air temperature and/or wind speed, have been compared. In this work, a simple approximation [16,41] was selected, because it simplifies the computation of the effect of changes of the different variables on PVpot:

$$T_{cell}(t) = a \cdot T_a(t) + b \cdot G(t) + c \cdot u_{wind}(t) + d, \quad (3)$$

where  $T_a$  is the air temperature and  $u_{wind}$  is the wind speed. The coefficients are [9]:  $a = 1.08$ ,  $b = 0.0226^\circ\text{C m}^2 \text{ W}^{-1}$ ,  $c = -1.83^\circ\text{C s m}^{-1}$  and  $d = 4.22^\circ\text{C}$ . This linear model is not suitable for wind speeds higher than  $10 \text{ ms}^{-1}$ , which are only common in the ocean areas between the islands [34], because it produces unrealistic low

module temperatures.

Rearranging equations (1)–(3) and replacing all the constants by their corresponding values, a simplified expression for PV potential can be obtained:

$$PVpot = G(c_1 + c_2 \cdot u_{wind} + c_3 \cdot G + c_4 \cdot T_a), \quad (4)$$

with  $c_1 = [1 + \gamma(d - T_{STC})]/G_{STC} = 1.1039 \times 10^{-3} \text{ m}^2 \text{ W}^{-1}$ ,  $c_2 = \gamma c/G_{STC} = 9.15 \times 10^{-6} \text{ s m W}^{-1}$ ,  $c_3 = \gamma b/G_{STC} = -1.13 \times 10^{-7} \text{ m}^4 \text{ W}^{-2}$  and  $c_4 = \gamma a/G_{STC} = -5.4 \times 10^{-6}^\circ\text{C}^{-1} \text{ m}^2 \text{ W}^{-1}$ . From this expression, changes in PVpot ( $\Delta PVpot$ ) due to changes in  $u_{wind}$ ,  $G$  and  $T_a$  can be calculated:

$$\Delta PVpot = \Delta G(c_1 + c_2 u_{wind} + c_3 \Delta G + 2c_3 G + c_4 T_a) + c_2 G \Delta u_{wind} + c_4 G \Delta T_a + c_2 \Delta G \Delta u_{wind} + c_4 \Delta G \Delta T_a. \quad (5)$$

To compute the relative contributions from  $\Delta u_{wind}$ ,  $\Delta T_a$  and  $\Delta G$ , the changes in PVpot were calculated keeping the remaining variables constant at their annual or seasonal means for the present period (1995–2004). For example, taking  $\Delta G = 0$  and  $\Delta u_{wind} = 0$ , the contribution of  $T_a$  can be estimated, keeping in mind that to fully isolate the contribution of each single variable is not possible due to the last two terms of the equation, where the changes of two variables are multiplied.

## 2.3. Observational data

The daily solar irradiance obtained from WRF simulations for the present period (1995–2004) was compared with observational data. Two kinds of datasets were used, the first one being two databases obtained from satellite measurements, and the second, ground measurements corresponding to several weather stations.

One of the databases is HelioClim-1 [42], which contains the daily values of the solar radiation reaching the ground and is freely accessible through the SoDa Service ([www.soda-is.com](http://www.soda-is.com)). This database was created from Meteosat images using the Heliosat-2 algorithm [43,44]. The other database is that provided by the project ADRASE ([www.adrase.com](http://www.adrase.com)). In this case, geostationary satellites images are also used, applying a methodology [45] developed in the Spanish CIEMAT (Research Centre for Energy, Environment and Technology). In both cases, the spatial resolution over the studied area is around 5 km.

Observational records of 7 stations belonging to AEMET (Spanish Meteorological Agency) were also used (Fig. 3). They correspond to airport stations, except the IZA station that is located in the Izaña Atmospheric Observatory at 2371 m asl and SCT, located in Santa Cruz city at 35 m asl. The daily solar irradiance was not available for the seven stations for the full studied period (1995–2004), but it was available for recent years, as summarised in Fig. 4. However, the daily sunshine duration was available for the whole period, 1995–2017, and for all the sites. For this reason, a method was used to transform sunshine duration to solar radiation, using the relationship used in previous studies [17,46]. This relationship can be expressed as:

$$f_{clear} = \left( \frac{\bar{H}}{\bar{H}_{clear}} \right)^2, \quad (6)$$

where  $\bar{H}$  is the monthly-mean of daily horizontal surface irradiation,  $\bar{H}_{clear}$  is the corresponding mean value of daily clear sky, cloud-free, irradiation, and  $f_{clear}$  is the time fraction of clear sky, that for a specific month and location is equivalent to the sunshine fraction ( $S$ ):



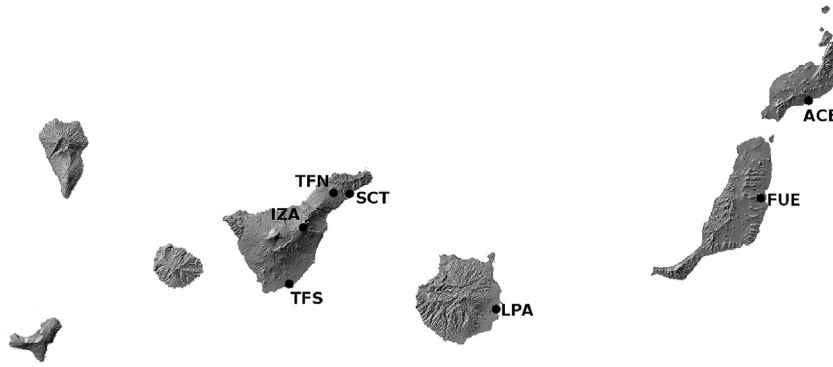


Fig. 3. Location of the stations used for WRF solar irradiance results assessment.

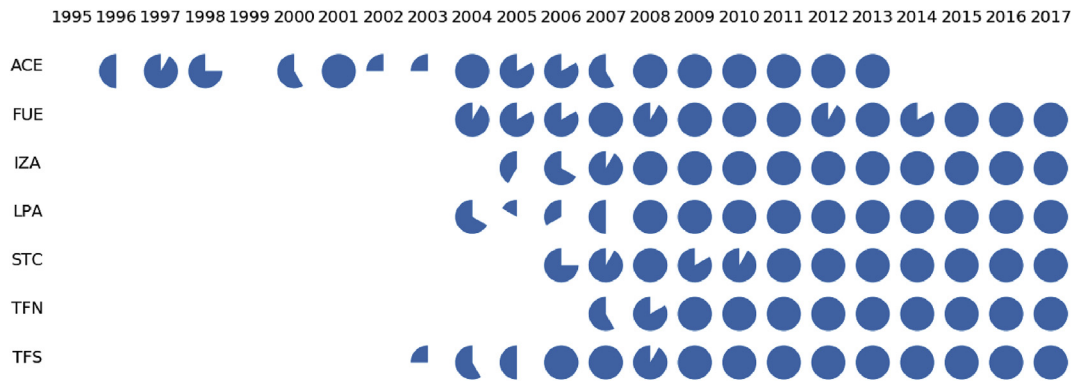


Fig. 4. Percentage of daily solar irradiance data available for each site and year. A full circle indicates full availability and an empty space indicates that data are not available for that year.

$$f_{clear} \equiv S = \frac{SD}{N}, \quad (7)$$

where  $SD$  is the average monthly sunshine duration and  $N$  is the average monthly day length, given by:

$$N = \frac{2}{15} \cos^{-1}(-\tan\phi \tan\delta), \quad (8)$$

with  $\phi$  the latitude of the site in degrees and  $\delta$  the declination of the sun, also in degrees, that can be estimated by:

$$\delta = 23.45 \sin\left(360 \frac{284 + n}{365}\right), \quad (9)$$

where  $n$  is the day of the year, starting on 1st January. Thus, for a particular site and month,  $\bar{H}$  can be computed as:

$$\bar{H} = \bar{H}_{clear} \left(\frac{SD}{N}\right)^{1/2}. \quad (10)$$

$\bar{H}_{clear}$  is not available from observations, but it was determined for every site and month of the year using those periods of the recent years (2004–2013 for ACE and 2009–2017 for the rest of the sites) for which both daily horizontal surface radiation and sunshine duration were available. Using these values for  $\bar{H}_{clear}$ , the solar irradiance was computed for all those months of the interval 1995–2008, which includes the study period, filling the gaps in the data series. This methodology was evaluated by comparing computed and measured irradiances for those months of this time

interval when the two variables were available, finding that the root mean square error in computed  $\bar{H}$  compared with observed values is 3.3%, computed as the average for all the seven locations.

#### 2.4. Assessment of changes in photovoltaic resources

Annual and seasonal changes in daily mean irradiation and  $PV_{pot}$  for the two selected future decades (2045–2054 and 2090–2099) and the two emission scenarios (RCP4.5 and RCP8.5) with respect to the present decade (1995–2004) were computed. To establish the statistical significance of the obtained changes, a non parametric technique was used. In this work, a moving block bootstrap algorithm, which takes into account the effects of data autocorrelation, was implemented [47] (the Python code is available at <https://bitbucket.org/jcperez/solar/src>). Based on previous evaluations of this method for other variables in the Canary Islands [33,34], the autoregressive-moving average process, of order 1 in both contributions, that is ARMA(1,1), has been selected and evaluated for the variables used in this work. For each grid point of the innermost domain, the corresponding ARMA(1,1) model was computed using daily time series and, based on its characteristics, the block length for the bootstrap test and the adjusted data variance for the test statistic were calculated [47].

### 3. Results

In this section, the WRF simulation results for the present period are evaluated and the projected changes in PV resources for the two future periods and two greenhouse gases emission scenarios are described.

### 3.1. Monthly-mean daily solar irradiation assessment

The WRF simulation results for the present period were compared with observational data from the seven available stations, taking the closest grid point of the innermost domain. The corresponding values of the Helioclim-1 and ADRASE databases were also used. A summary of these comparisons, based on monthly-mean values, is summarized in Fig. 5. The computed values clearly overestimate observational irradiances, with mean

biases ranging from 2 to 16% (approximately between  $-1$  and  $20\%$  if the error in obtaining solar irradiance from ground measured sunshine duration, as explained in Section 2.3, is considered) The overestimation of solar radiation is a common problem in GCMs [48–51] and also in regional models [16,52]. A similar mean bias,  $16\%$ , was obtained for the whole Spanish peninsula also using the WRF model [52].

As previously mentioned, while optical properties of the atmosphere, mainly due to aerosols, affect the solar irradiance, clouds are

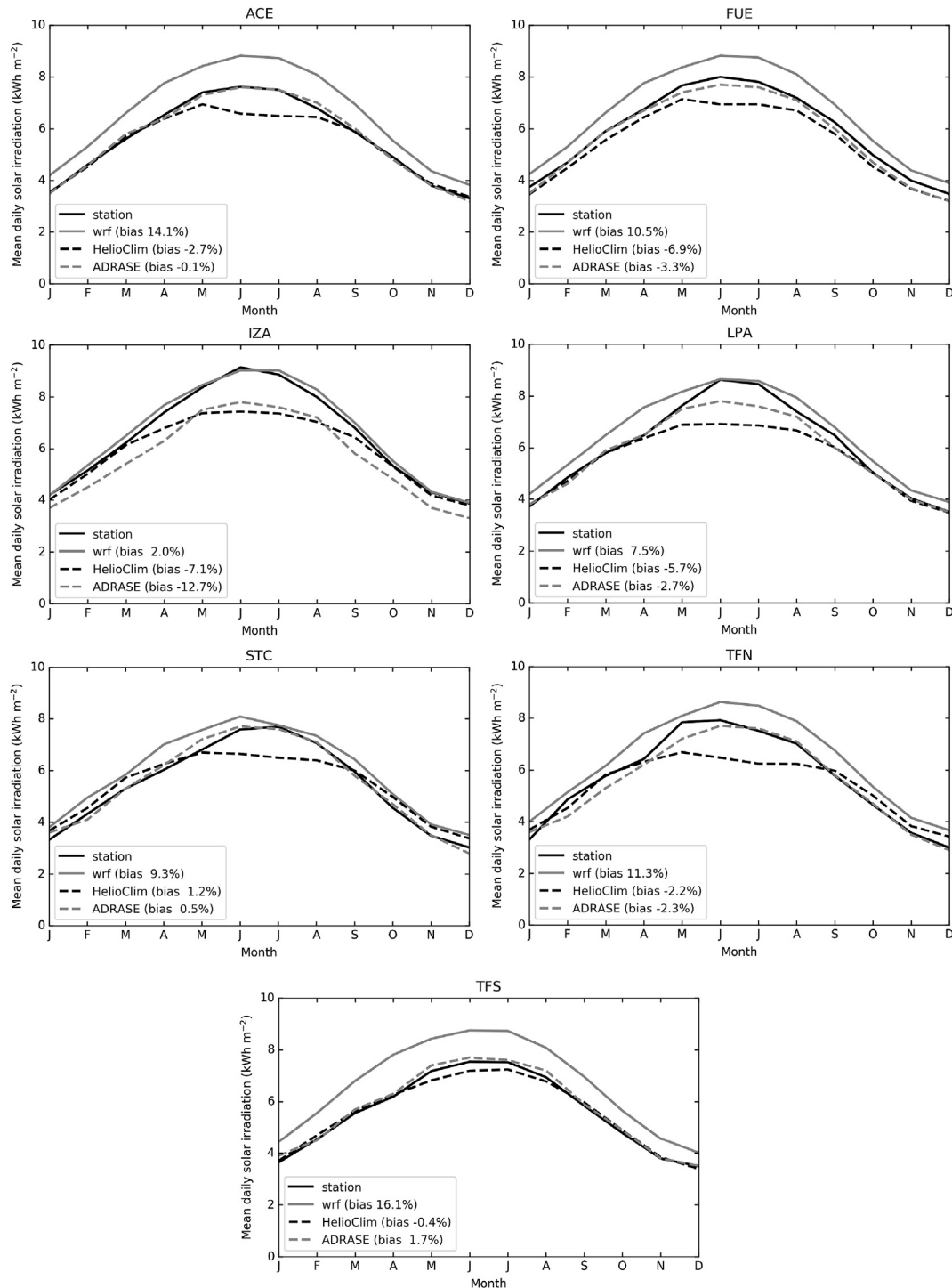
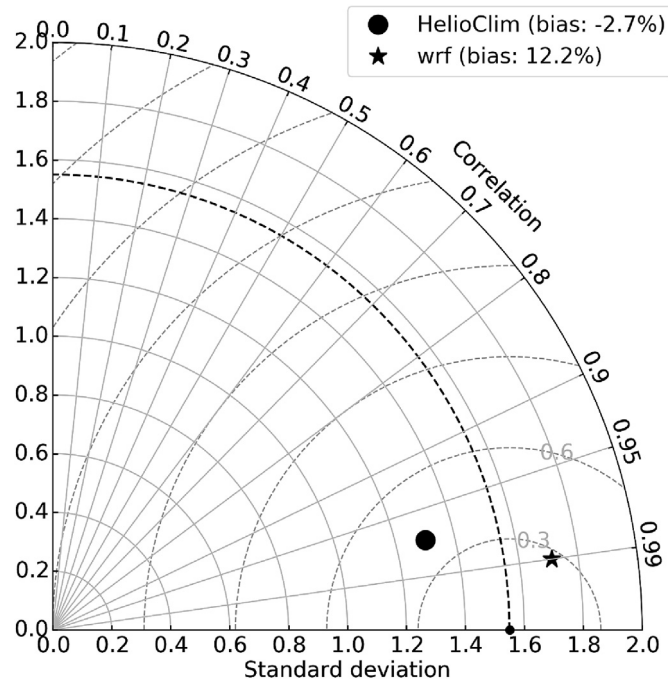


**Fig. 5.** Comparison of monthly mean daily irradiation for the period 1995–2004 obtained from weather stations, Helioclim-1 and ADRASE databases and computed by the WRF model. The bias, in percentage, for each of the seven sites is indicated in the corresponding plot legend.

responsible for the largest uncertainties in irradiance simulation. Therefore, to take into account the behavior and distribution of cloud cover, both databases were used to assess WRF simulated irradiances. The observational data were interpolated to the same grid used in WRF using bilinear interpolation. A total of 264 grid-points, which correspond to land areas, were used. To summarize, the results of the comparison are displayed in a graphical way, using the diagram proposed by Taylor [53], selecting the ADRASE database as the reference, or ground truth. The main statistical results of the total spatial and temporal variability [54] of monthly irradiance obtained from the HelioClim-1 database and WRF simulations compared to ADRASE data are presented in Fig. 6. The bias is indicated in the plot legend. From these results, the good behavior of the WRF simulation for the historical period is clear. Its spatial-temporal correlation coefficient, for the land gridpoints, compared with the ADRASE data is around 0.99, larger than for HelioClim-1 observations. CRMSE and variance are also slightly better for WRF results. Hence, the uncertainties in the spatial distribution and temporal behavior of WRF simulated irradiances are similar to the differences between both observational databases. However, the general overestimation of irradiance by WRF simulation is evident, and similar to other previously mentioned studies. As analysed in a prior work [52], the bias in modeled surface irradiation using WRF cannot only be explained by a hypothetical bias in aerosol optical depth, or in the radiative effect of atmospheric gases. This overestimation is mainly due to an underestimation of the cloud cover and/or an underestimation of the radiative impact of the simulated clouds.

### 3.2. Present PV resource and future projections

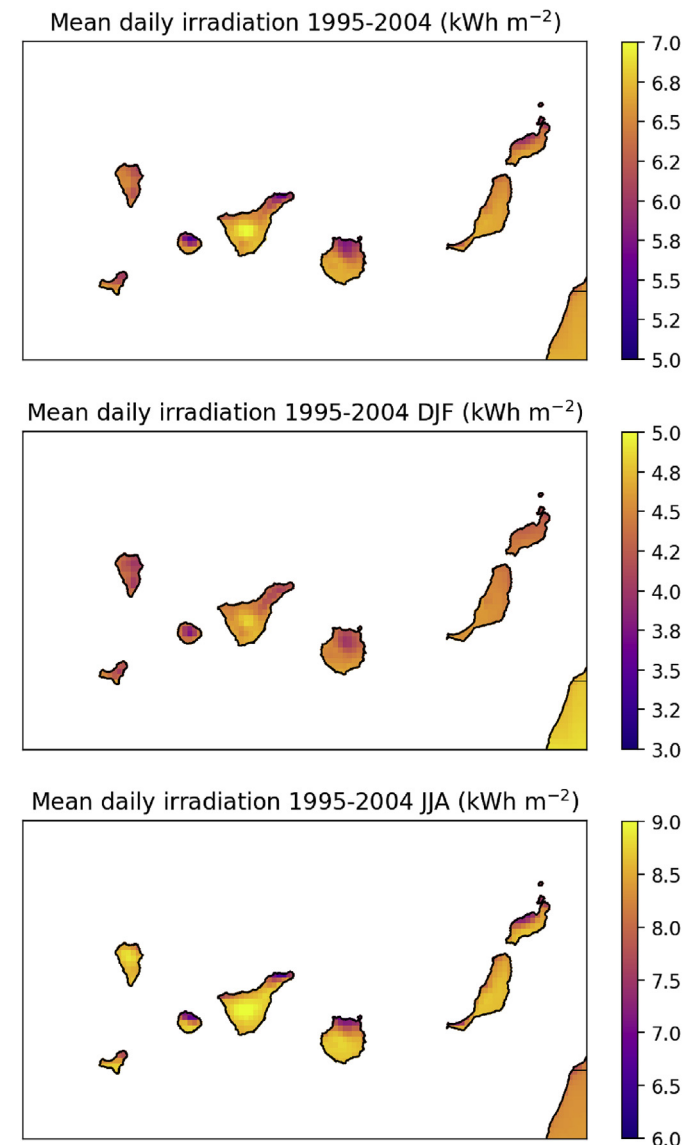
The present climatology of daily irradiation for the Canary



**Fig. 6.** Taylor diagram illustrating the comparison between the different observed/simulated data. The standard deviation of the monthly mean ADRASE irradiances is represented by a solid circle on the abscissa. The other two symbols, which represent the data of HelioClim-1 database and WRF simulations, respectively, are positioned such that their standard deviation (%) is the radial distance from the origin, their correlation coefficient with respect to the ADRASE data is the cosine of the azimuthal angle, and their centred root-mean-square (CRMS) difference is the distance to the point on the abscissa. The corresponding biases (%) are indicated in the legend.

Islands, obtained from WRF simulations, is summarised in Fig. 7. The annual-mean values show the effects of the orography, with higher values in the top areas of the mountainous islands, up to  $7 \text{ kWh m}^{-2}$ , and the lowest values in the northern part of these islands, less than  $6 \text{ kWh m}^{-2}$ , with more cloud cover. The contrast between the northern and southern areas is larger during summer, more than  $2 \text{ kWh m}^{-2}$  difference between both regions, when the persistent trade winds and the subsidence inversion create an optimal environment for the development of marine stratocumulus, which cover the north facing coasts but are blocked by high mountains.

Projected mean annual changes in daily irradiation for the two future decades with respect to the present decade are small and not statistically significant, so the corresponding maps were not included. The mean future changes in daily irradiation for winter and summer are presented in Fig. 8. There is a clear difference in behavior between the two seasons. A future general increase in solar radiation can be observed during winter, due to a decrease in cloud cover. As can be expected, the largest and most significant



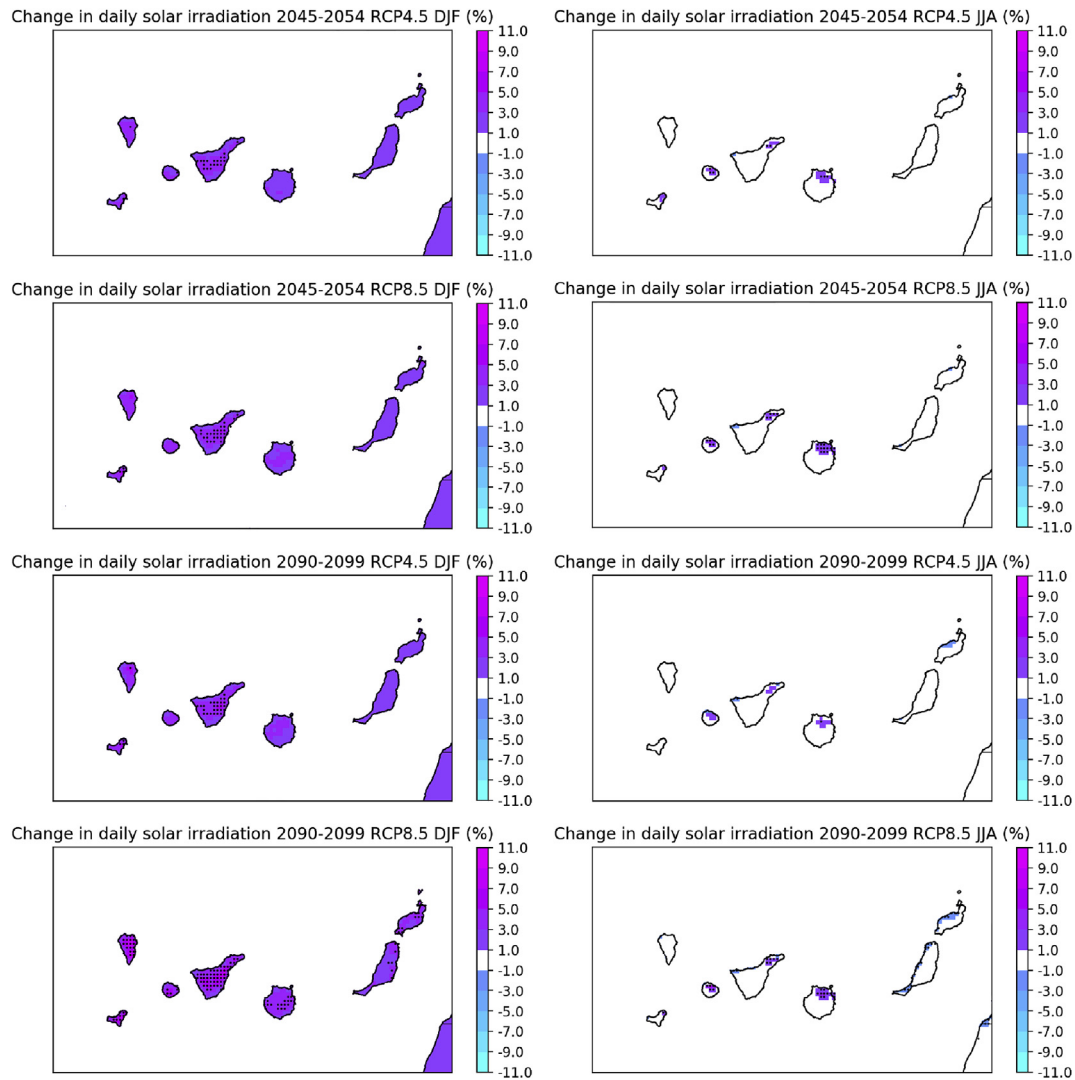


**Fig. 8.** Mean daily irradiation differences (in percentage) between future simulations and present for two periods: at the middle of the century (2045–2054) and at the end (2090–2099). Two greenhouse emission scenarios have been used: RCP4.5 and RCP8.5. The results correspond to two different seasons, winter-DJF (left) and summer-JJA (right). Black dots indicate those areas where the changes are statistically significant ( $p < 0.05$ ).

changes correspond to the end of the century and were obtained using the RCP8.5 scenario, which specifies a larger increment in GHGs. In this case, the expected change is around 7% in those areas which show statistical significance. On the other hand, the computed changes for summer are localized, with an increase of solar irradiation, around 5% at the end of the century, in the areas most affected by stratocumulus in the highest (western) islands, due to less stratocumulus cloud cover, and a decrease of solar radiation, of the same order, in the northern coast of the eastern islands, which is statistically significant only at the end of the century.

Although the variation of solar radiation is the main factor affecting the changes in the photovoltaic energy generation, other previously mentioned factors must be also taken into account, such as changes in air temperature and/or in wind speed. Thus, Figs. 9 and 10 show the simulated changes for PVpot in winter and summer, respectively, and the relative contribution of each of these variables. For winter (Fig. 9), a general rise in photovoltaic potential was obtained. However, the differences are only statistically significant in a few locations, and around 5% at the end of the century. Changes in PVpot are dominated by the increase in solar irradiance. The air temperature rise induces a decrease in PV panel efficiency

and, therefore, in PVpot, but this contribution is smaller in magnitude, less than half the PVpot increase due to solar radiation changes. Finally, the contribution of changes in wind speed is lower than those produced by the other two variables, and is only discernible in small areas and for the RCP8.5 scenario.

As discussed earlier, changes in daily solar irradiation are smaller and more localized in summer, so they are not able to counteract the decline in photovoltaic potential due to the increase in air temperature. This effect dominates in almost all the territory, except in small areas, where the reduction in the coverage of the marine stratocumulus is enough to provoke a net increase of PVpot. At the end of the century and for the scenario corresponding to a greater content of GHGs (RCP8.5), the loss in PVpot is larger than 5% in most areas. Similar results were obtained by for Spain [16]. In summer, the reduction in PVpot is governed by the increase in air temperature, except for the northern Spanish coast, where this increase is lower and then, the rise in solar irradiation prevails.

#### 4. Conclusions and discussion

Regional climate modeling is essential to project future changes in regions with complex orography, as is the case of the Canarian



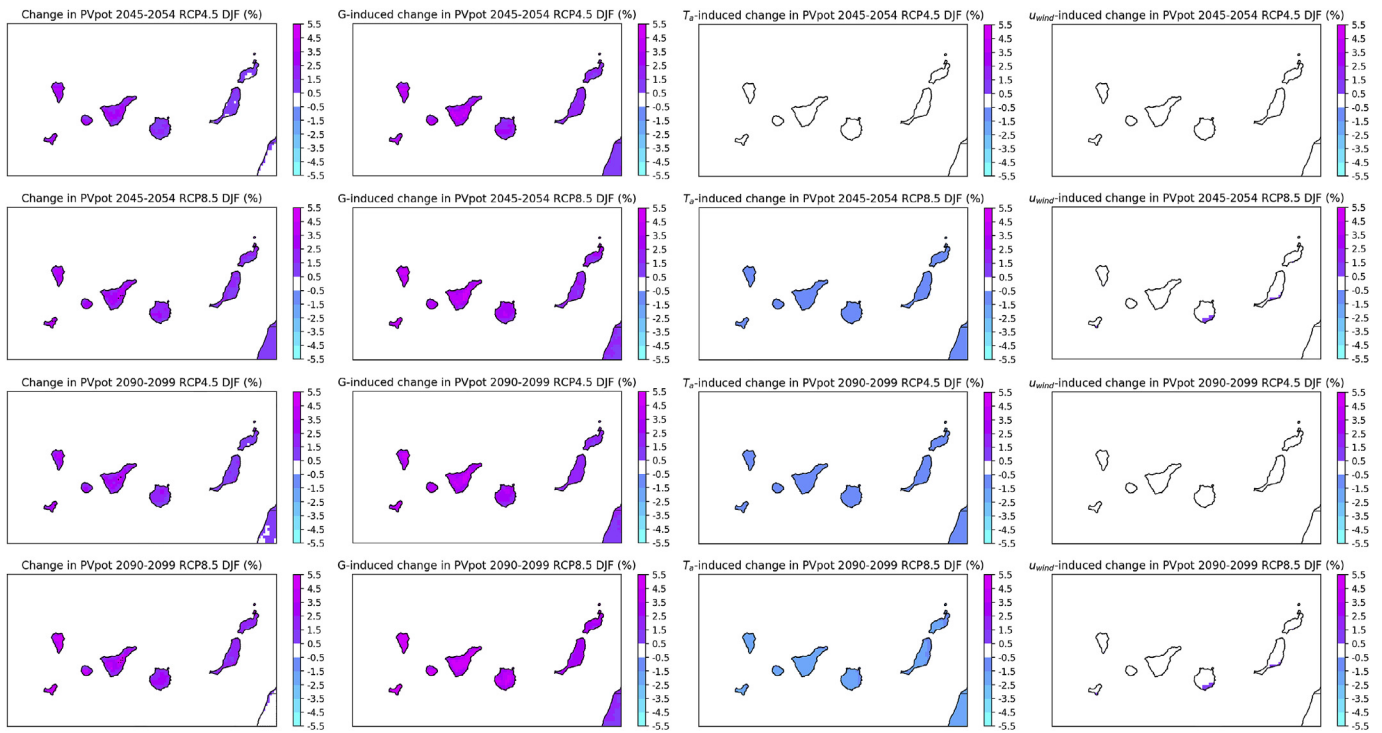


**Fig. 9.** Projected mean changes in PVpot (left column) for winter, computed for the two future decades (2045–2054 and 2090–2099) and both emission scenarios (RCP4.5 and RCP8.5). Black dots indicate those areas where the changes are statistically significant ( $p < 0.05$ ). The changes in PVpot that would be induced by the variations in solar irradiation alone (second column), air temperature alone (third column) or wind speed alone (right column) are also displayed.

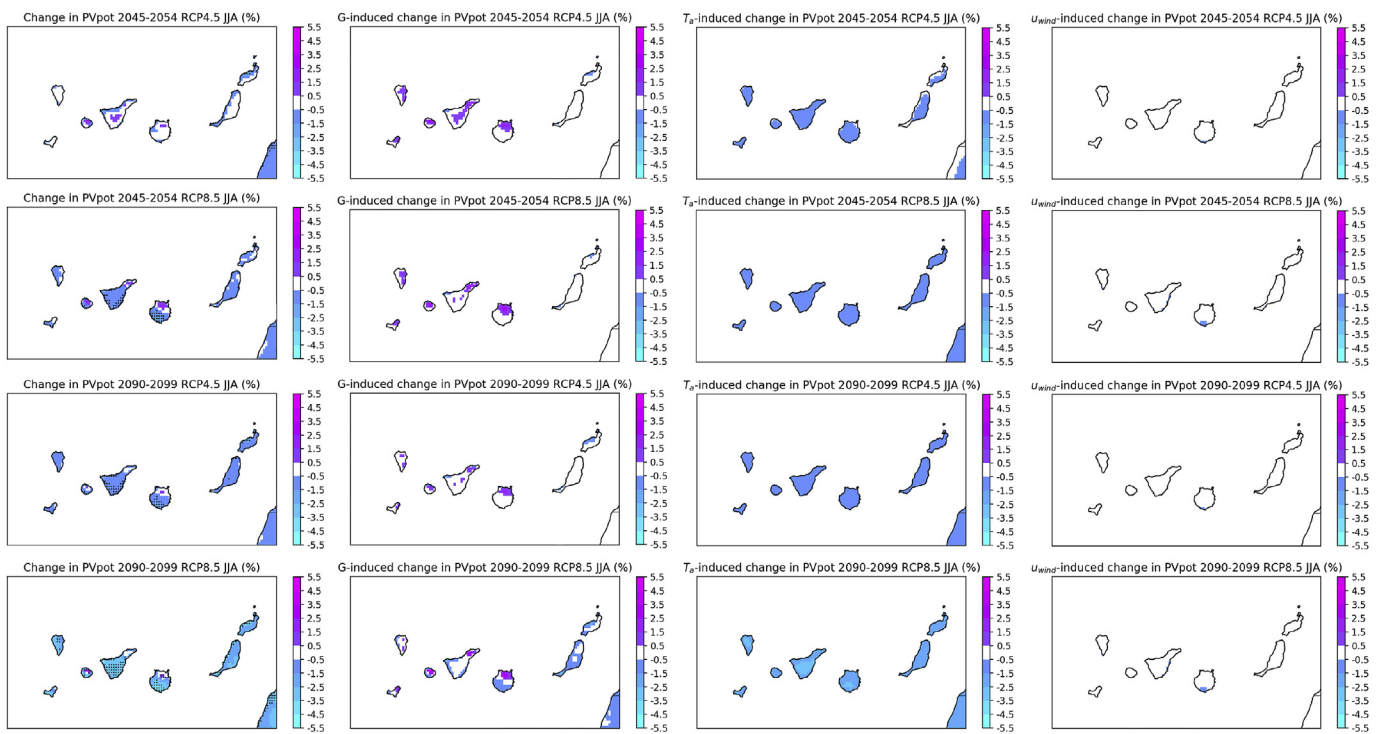


**Fig. 10.** Same as in Fig. 9 but the summer season.

Archipelago. In this work the pseudo-global warming approach was used to obtain the projected changes in PV resources in this archipelago. This choice allowed us to reduce the computational cost of the high resolution simulations required in this area and to avoid

the problem of global climate model biases in the present period. Although this methodology is inadequate to assess the possible changes in extreme events, the changes in absolute solar irradiation and PV potential can be studied.

Even though no statistically significant changes were found in annual mean photovoltaic potential for the two future decades with respect to the present decade, significant changes were observed at seasonal scale. In addition, the behavior is very different between winter and summer. During winter, a general increase in PVpot is expected, driven by the rise of solar radiation, that is due, in turn, to a decrease in cloud cover. On the contrary, during the summer a reduction in the photovoltaic potential is expected, which is due to an increase of the temperature, affecting the efficiency of energy production of the photovoltaic panels. The only exception to this reduction occurs in very localized areas of the north coast of the most prominent islands, where the effect of the decrease in the stratocumulus coverage prevails and, therefore, the increase of solar radiation.

The possible modifications in PV resources due to climate change, as those presented in this study, and not only past observational data and model simulations, should be taken into account in the planning of new PV plants or the development of the current ones. Although the lifespan of the PV modules is generally considered to be around 30–40 years [55], the life span of other energy infrastructures is longer, such as the transmission lines, 40–75 years [7]. Moreover, the scarcity of available ground to construct energy infrastructures in small islands and the difficulty to obtain the corresponding permissions, make the decisions about the convenient locations an important aspect in PV planning, a possible refurbishing of energy plants in the future in the future being usually more feasible than a relocation of them. This is especially important in the Canary Islands, where 41% of the territory has been declared as natural protected areas [56]. Due to these considerations, the climate impacts for the whole present century have been considered.

Despite the relevance of the results shown in this work, there are some aspects that can be considered in future works to improve the accuracy of the projections. Although the bias in solar irradiance found in this study is similar, and even lower, to those obtained in previous studies, a comprehensive study of the cloud cover in the archipelago and the ability of different parameterizations included in WRF to accurately simulate it, can be carried out to diminish this bias. In addition, the change in atmospheric aerosols composition and concentration was not directly taken into account for the regional simulations. They were only considered in the GCMs used to compute the boundary conditions for the WRF runs. In any case, the inclusion of the aerosols in the simulations is more relevant in the calculation of the direct normal radiance, applied to concentrated solar power systems, not to PV systems, for which the global horizontal component is computed [57].

Another important aspect to keep in mind is the expected improvement of solar panel efficiencies in the future, which could overwhelm climate change induced impacts. Although the PV potential does not account for the energy conversion efficiency, monocrystalline silicon solar panels were assumed in this work to characterize the variation of their efficiency with temperature. As the crystalline silicon is a mature technology, efficiency improvements have been relatively small in the last decade. However, the efficiencies of other technologies and materials, such as gallium arsenide or perovskite, have been improved during last years [58]. Moreover, some emerging technologies try to overtake the Shockley and Queisser limit [59] by using the process of multiple exciton generation, by up- or down-conversion of incident radiation or by limiting the range of radiative emission angles [58]. If other types of solar panels were considered, their temperature coefficients of efficiency should be also taken into account, since they strongly depend on the considered material [60,61]. The analysis of the different technologies that will be used in the future and the effect of climate change on each of them is out of the scope of this study.

## Acknowledgement

The authors acknowledge the MINECO (Ministry of Economy and Competitiveness, Spain) for the Project CGL2015-67508-R and Fundación CajaCanarias for the Project CLI05-2016. The weather station's data were obtained from the Meteorological State Agency of Spain (AEMET), the ERA-Interim data were provided by the European Centre for Medium-Range Weather Forecasts (ECMWF), the HelioClim-1 data were downloaded from the SoDa Service portal and the ADRASE data were obtained from the project webpage. We also acknowledge the World Climate Research Programme's Working Group on Coupled Modelling, which is responsible for CMIP, and we thank the climate modeling institutions (listed in Table 1) for producing and making their model output available. For CMIP the U.S. Department of Energy's Program for Climate Model Diagnosis and Intercomparison provides coordinating support and led development of software infrastructure in partnership with the Global Organization for Earth System Science Portals. The WRF simulations performed in this study were managed by WRF4G.

## References

- [1] Intergovernmental Panel on Climate Change, in: *Climate Change 2013 - the Physical Science Basis*, Cambridge University Press, Cambridge, 2013, <https://doi.org/10.1017/cbo9781107415324>.
- [2] O. Edenhofer, R. Madruga, Y. Sokona, K. Seyboth, P. Matschoss, S. Kadner, T. Zwickel, P. Eickemeier, G. Hansen, S. Schlmer, C. Stechow, *Renewable Energy Sources and Climate Change Mitigation: Special Report of the Intergovernmental Panel on Climate Change*, 2011, pp. 1–1075.
- [3] L. Dubus, *Weather and Climate and the Power Sector: Needs, Recent Developments and Challenges*, Springer New York, New York, NY, 2014, pp. 379–398, [https://doi.org/10.1007/978-1-4614-9221-4\\_18](https://doi.org/10.1007/978-1-4614-9221-4_18).
- [4] J.-C. Ciscar, P. Dowling, Integrated assessment of climate impacts and adaptation in the energy sector, *Energy Econ.* 46 (2014) 531–538, <https://doi.org/10.1016/j.eneco.2014.07.003>.
- [5] R. Schaeffer, A.S. Szklo, A.F.P. de Lucena, B.S.M.C. Borba, L.P.P. Nogueira, F.P. Fleming, A. Troccoli, M. Harrison, M.S. Boulahya, Energy sector vulnerability to climate change: a review, *Energy* 38 (1) (2012) 1–12, <https://doi.org/10.1016/j.energy.2011.11.056>.
- [6] J.W. Zillman, *Weather and Climate Information Delivery within National and International Frameworks*, Springer New York, New York, NY, 2014, pp. 201–219, [https://doi.org/10.1007/978-1-4614-9221-4\\_9](https://doi.org/10.1007/978-1-4614-9221-4_9).
- [7] J. Ebinger, W. Vergara, *Climate Impacts on Energy Systems: Key Issues for Energy Sector Adaptation*, no. 2271, World Bank Publications, The World Bank, 2011.
- [8] F. Mavromatakis, G. Makrides, G. Georgiou, A. Pothrakakis, Y. Franghiadakis, E. Drakakis, E. Koudoumas, Modeling the photovoltaic potential of a site, *Renew. Energy* 35 (7) (2010) 1387–1390, <https://doi.org/10.1016/j.renene.2009.11.010>.
- [9] F. Mavromatakis, E. Kavoussanaki, F. Vignola, Y. Franghiadakis, Measuring and estimating the temperature of photovoltaic modules, *Sol. Energy* 110 (2014) 656–666, <https://doi.org/10.1016/j.solener.2014.10.009>.
- [10] REE, *Renewable Energy in the Spanish Electricity System 2016*, Tech. rep., Red Eléctrica de España, Madrid, Spain, June 2017 [http://www.ree.es/sites/default/files/11\\_PUBLICACIONES/Documentos/Renewable-2016.pdf](http://www.ree.es/sites/default/files/11_PUBLICACIONES/Documentos/Renewable-2016.pdf).
- [11] REE, *Red Eléctrica de España*, accessed 2018-06-30 (2018). URL <http://www.ree.es>.
- [12] J.A. Crook, L.A. Jones, P.M. Forster, R. Crook, Climate change impacts on future photovoltaic and concentrated solar power energy output, *Energy Environ. Sci.* 4 (2011) 3101–3109, <https://doi.org/10.1039/C1EE01495A>.
- [13] M. Wild, D. Folini, F. Henschel, N. Fischer, B. Müller, Projections of long-term changes in solar radiation based on CMIP5 climate models and their influence on energy yields of photovoltaic systems, *Sol. Energy* 116 (2015) 12–24, <https://doi.org/10.1016/j.solener.2015.03.039>.
- [14] C. Fant, C.A. Schlosser, K. Strzepek, The impact of climate change on wind and solar resources in southern Africa, *Appl. Energy* 161 (2016) 556–564, <https://doi.org/10.1016/j.apenergy.2015.03.042>.
- [15] F. Giorgi, L.O. Mearns, Introduction to special section: regional climate modeling revisited, *J. Geophys. Res.: Atmos.* 104 (D6) (1999) 6335–6352, <https://doi.org/10.1029/98JD02072>.
- [16] S. Jerez, I. Tobin, R. Vautard, J.P. Montávez, J.M. López-Romero, F. Thais, B. Bartok, O.B. Christensen, A. Colette, M. Déqué, G. Nikulin, S. Kotlarski, E. van Meijgaard, C. Teichmann, M. Wild, The impact of climate change on photovoltaic power generation in Europe, *Nat. Commun.* 6 (2015), <https://doi.org/10.1038/ncomms10014>.
- [17] D. Burnett, E. Barbour, G.P. Harrison, The UK solar energy resource and the impact of climate change, *Renew. Energy* 71 (2014) 333–343, <https://doi.org/10.1016/j.renene.2014.05.034>.

- [18] I. S. Panagea, I. K. Tsanis, A. G. Koutroulis, M. G. Grillakis, Climate change impact on photovoltaic energy output: the case of Greece, *Adv. Meteorol.* <https://doi.org/10.1155/2014/264506>.
- [19] W.C. Skamarock, J.B. Klemp, J. Dudhia, D.O. Gill, M. Barker, K.G. Duda, X.Y. Huang, W. Wang, J.G. Powers, A Description of the Advanced Research WRF Version 3, Tech. rep., National Center for Atmospheric Research, 2008.
- [20] F. Kimura, A. Kitoh, Downscaling by Pseudo Global Warming Method, The Final Report of IPCC AR 4346, 2007.
- [21] T. Sato, F. Kimura, A. Kitoh, Projection of global warming onto regional precipitation over Mongolia using a regional climate model, *J. Hydrol.* 333 (1) (2007) 144–154, <https://doi.org/10.1016/j.jhydrol.2006.07.023>.
- [22] H. Kawase, T. Yoshikane, M. Hara, F. Kimura, T. Yasunari, B. Ailikun, H. Ueda, T. Inoue, Intermodel variability of future changes in the Baiu rainband estimated by the pseudo global warming downscaling method, *J. Geophys. Res.* 114 (2009), <https://doi.org/10.1029/2009JD011803>.
- [23] A. González, F.J. Expósito, J.C. Pérez, J.P. Díaz, D. Taima, Verification of precipitable water vapour in high-resolution WRF simulations over a mountainous archipelago, *Q. J. R. Meteorol. Soc.* 139 (677) (2013) 2119–2133, <https://doi.org/10.1002/qj.2092>.
- [24] J. Pérez, J. Díaz, A. González, J. Expósito, F. Rivera-López, D. Taima, Evaluation of WRF parameterizations for dynamical downscaling in Canary Islands, *J. Clim.* (27) (2014) 5611–5631, <https://doi.org/10.1175/JCLI-D-13-00458.1>.
- [25] W.D. Collins, P.J. Rasch, B.A. Boville, J.J. Hack, J.R. McCaa, D.L. Williamson, J.T. Kiehl, B. Briegleb, C. Bitz, S.-J. Lin, et al., Description of the NCAR Community Atmosphere Model (CAM 3.0), 2004.
- [26] W.D. Collins, P.J. Rasch, B.A. Boville, J.J. Hack, J.R. McCaa, D.L. Williamson, B.P. Briegleb, C.M. Bitz, S.-J. Lin, M. Zhang, The formulation and atmospheric simulation of the community atmosphere model version 3 (CAM3), *J. Clim.* 19 (11) (2006) 2144–2161, <https://doi.org/10.1175/JCLI3760.1>.
- [27] J.S. Kain, J.M. Fritsch, A one-dimensional entraining/detraining plume model and its application in convective parameterization, *J. Atmos. Sci.* 47 (23) (1990) 2784–2802, doi:0.1175/1520-0469(1990)047<2784:AODEPM>2.0.CO;2.
- [28] S.-Y. Hong, Y. Noh, J. Dudhia, A new vertical diffusion package with an explicit treatment of entrainment processes, *Mon. Weather Rev.* 134 (9) (2006) 2318–2341, <https://doi.org/10.1175/MWR3199.1>.
- [29] F. Chen, J. Dudhia, Coupling an advanced land surface-hydrology model with the Penn State-NCAR MM5 modeling system. Part I: model implementation and sensitivity, *Mon. Weather Rev.* 129 (4) (2001) 569–585, [https://doi.org/10.1175/1520-0493\(2001\)129<0569:CAALSH>2.0.CO;2](https://doi.org/10.1175/1520-0493(2001)129<0569:CAALSH>2.0.CO;2).
- [30] K.-S.S. Lim, S.-Y. Hong, Development of an effective double-moment cloud microphysics scheme with prognostic cloud condensation nuclei (CCN) for weather and climate models, *Mon. Weather Rev.* 138 (5) (2010) 1587–1612, <https://doi.org/10.1175/2009MWR2968.1>.
- [31] W.-D. Chen, F. Cui, H. Zhou, H. Ding, D.-X. Li, Impacts of different radiation schemes on the prediction of solar radiation and photovoltaic power, *Atmos. Ocean. Sci. Lett.* 10 (6) (2017) 446–451, <https://doi.org/10.1080/16742834.2017.1394780>.
- [32] A. Montornès, B. Codina, J. Zack, A Discussion about the Role of Shortwave Schemes on Real WRF-ARW Simulations. Two Case Studies: Cloudless and Cloudy Sky, *Tethys*, 2015, pp. 13–31, <https://doi.org/10.3369/tethys.2015.12.02>.
- [33] F.J. Expósito, A. González, J.C. Pérez, J.P. Díaz, D. Taima, High-resolution future projections of temperature and precipitation in the canary islands, *J. Clim.* 28 (19) (2015) 7846–7856, <https://doi.org/10.1175/JCLI-D-15-0030.1>.
- [34] A. González, J.C. Pérez, J.P. Díaz, F.J. Expósito, Future projections of wind resource in a mountainous archipelago, Canary Islands, *Renew. Energy* 104 (2017) 120–128, <https://doi.org/10.1016/j.renene.2016.12.021>.
- [35] D. Dee, S. Uppala, A. Simmons, P. Berrisford, P. Poli, S. Kobayashi, U. Andrae, M. Balmaseda, G. Balsamo, P. Bauer, et al., The ERA-Interim reanalysis: configuration and performance of the data assimilation system, *Q. J. Roy. Meteorol. Soc.* 137 (656) (2011) 553–597, <https://doi.org/10.1002/qj.828>.
- [36] K.E. Taylor, R.J. Stouffer, G.A. Meehl, An overview of CMIP5 and the experiment design, *Bull. Am. Meteorol. Soc.* 93 (4) (2012) 485–498, <https://doi.org/10.1175/BAMS-D-11-00094.1>.
- [37] D.P. Van Vuuren, J. Edmonds, M. Kainuma, K. Riahi, A. Thomson, K. Hibbard, G.C. Hurtt, T. Kram, V. Krey, J.-F. Lamarque, et al., The representative concentration pathways: an overview, *Climatic Change* 109 (2011) 5–31, <https://doi.org/10.1007/s10584-011-0148-z>.
- [38] WMO, Guide to Climatological Practices/World Meteorological Organization, 2011th Edition, World Meteorological Organization, Geneva, Switzerland, 2011. [http://www.wmo.int/pages/prog/wcp/ccl/guide/documents/WMO\\_100\\_en.pdf](http://www.wmo.int/pages/prog/wcp/ccl/guide/documents/WMO_100_en.pdf).
- [39] H. Kawase, T. Yoshikane, M. Hara, B. Ailikun, F. Kimura, T. Yasunari, Downscaling of the climatic change in the Mei-yu rainband in East Asia by a pseudo climate simulation method, *SOLA* 4 (2008) 73–76, <https://doi.org/10.2151/sola.2008-019>.
- [40] A. Lauer, C. Zhang, O. Elison-Timm, Y. Wang, K. Hamilton, Downscaling of climate change in the Hawaii region using CMIP5 results: on the choice of the forcing fields, *J. Clim.* 26 (24) (2013) 10006–10030, <https://doi.org/10.1175/JCLI-D-13-00126.1>.
- [41] G. Tamizhmani, L. Ji, Y. Tang, L. Petacci, C. Osterwald, Photovoltaic module thermal/wind performance: long-term monitoring and model development for energy rating, in: NCPV and Solar Program Review Meeting 2003, 2003, pp. 936–939.
- [42] M. Lefèvre, P. Blanc, B. Espinar, B. Gschwind, L. Ménard, T. Ranchin, L. Wald, L. Saboret, C. Thomas, E. Wey, The HelioClim-1 database of daily solar radiation at Earth surface: an example of the benefits of GEOS data-CORE, *IEEE J. Select. Top. Appl. Earth Observ. Remote Sens.* 7 (5) (2014) 1745–1753, <https://doi.org/10.1109/JSTARS.2013.2283791>.
- [43] H.G. Beyer, C. Costanzo, D. Heinemann, Modifications of the Heliosat procedure for irradiance estimates from satellite images, *Sol. Energy* 56 (3) (1996) 207–212, [https://doi.org/10.1016/0038-092X\(95\)00092-6](https://doi.org/10.1016/0038-092X(95)00092-6).
- [44] B. Espinar, L. Ramirez, J. Polo, L. Zarzalejo, L. Wald, Analysis of the influences of uncertainties in input variables on the outcomes of the Heliosat-2 method, *Sol. Energy* 83 (2009) 1731–1741, <https://doi.org/10.1016/j.solener.2009.06.010>.
- [45] L.F. Zarzalejo, J. Polo, L. Martn, L. Ramrez, B. Espinar, A new statistical approach for deriving global solar radiation from satellite images, *Sol. Energy* 83 (4) (2009) 480–484, <https://doi.org/10.1016/j.solener.2008.09.006>.
- [46] H. Suehrcke, On the relationship between duration of sunshine and solar radiation on the Earth's surface: Ångström's equation revisited, *Sol. Energy* 68 (5) (2000) 417–425, [https://doi.org/10.1016/S0038-092X\(00\)00004-9](https://doi.org/10.1016/S0038-092X(00)00004-9).
- [47] D. Wilks, Resampling hypothesis tests for autocorrelated fields, *J. Clim.* 10 (1) (1997) 65–82.
- [48] P. Räisänen, H. Järvinen, Impact of cloud and radiation scheme modifications on climate simulated by the ECHAM5 atmospheric GCM, *Q. J. R. Meteorol. Soc.* 136 (652) (2010) 1733–1752, <https://doi.org/10.1002/qj.674>.
- [49] K. Van Weverberg, C.J. Morcrette, H.-Y. Ma, S.A. Klein, J.C. Petch, Using regime analysis to identify the contribution of clouds to surface temperature errors in weather and climate models, *Q. J. R. Meteorol. Soc.* 141 (693) (2015) 3190–3206, <https://doi.org/10.1002/qj.2603>.
- [50] M. Wild, Short-wave and long-wave surface radiation budgets in GCMs: a review based on the IPCC-AR4/CMIP3 models, *Tellus Dyn. Meteorol. Oceanogr.* 60 (5) (2008) 932–945, <https://doi.org/10.1111/j.1600-0870.2008.00342.x>.
- [51] M. Wild, D. Folini, C. Schär, N. Loeb, E.G. Dutton, G. König-Langlo, The global energy balance from a surface perspective, *Clim. Dynam.* 40 (11) (2013) 3107–3134, <https://doi.org/10.1007/s00382-012-1569-8>.
- [52] J.A. Ruiz-Arias, C. Arbizu-Barrena, F.J. Santos-Alamillos, J. Tovar-Pescador, D. Pozo-Vázquez, Assessing the surface solar radiation budget in the WRF model: a spatiotemporal analysis of the bias and its causes, *Mon. Weather Rev.* 144 (2) (2016) 703–711, <https://doi.org/10.1175/MWR-D-15-0262.1>.
- [53] K.E. Taylor, Summarizing multiple aspects of model performance in a single diagram, *J. Geophys. Res.: Atmos.* 106 (D7) (2001) 7183–7192, <https://doi.org/10.1029/2000JD900719>.
- [54] C. Covey, K.M. AchutaRao, U. Cubasch, P. Jones, S.J. Lambert, M.E. Mann, T.J. Phillips, K.E. Taylor, An overview of results from the coupled model Intercomparison project, *Global Planet. Change* 37 (12) (2003) 103–133, [https://doi.org/10.1016/S0921-8181\(02\)00193-5](https://doi.org/10.1016/S0921-8181(02)00193-5), evaluation, Intercomparison and Application of Global Climate Models.
- [55] M. Bazilian, I. Onyeji, M. Liebreich, I. MacGill, J. Chase, J. Shah, D. Gielen, D. Arent, D. Landfear, S. Zhengrong, Re-considering the economics of photovoltaic power, *Renew. Energy* 53 (2013) 329–338, <https://doi.org/10.1016/j.renene.2012.11.029>.
- [56] R.V. Bianchi, Tourism restructuring and the politics of sustainability: a critical view from the European periphery (The Canary Islands), *J. Sustain. Tourism* 12 (6) (2004) 495–529, <https://doi.org/10.1080/09669580408667251>.
- [57] I. Huber, L. Bugliaro, M. Ponater, H. Garny, C. Emde, B. Mayer, Do climate models project changes in solar resources? *Sol. Energy* 129 (2016) 65–84, <https://doi.org/10.1016/j.solener.2015.12.016>.
- [58] A. Polman, M. Knight, E.C. Garnett, B. Ehrler, W.C. Sinke, Photovoltaic materials: present efficiencies and future challenges, *Science* 352 (2016), <https://doi.org/10.1126/science.aad4424>.
- [59] W. Shockley, H.J. Queisser, Detailed balance limit of efficiency of pn junction solar cells, *J. Appl. Phys.* 32 (3) (1961) 510–519, <https://doi.org/10.1063/1.1736034>.
- [60] I. Audwinto, C. Leong, K. Sopian, S. Zaidi, Temperature dependences on various types of Photovoltaic (PV) panel, *IOP Conf. Ser. Mater. Sci. Eng.* 88 (1), <https://doi.org/10.1088/1757-899X/88/1/012066>.
- [61] T. Mishima, M. Taguchi, H. Sakata, E. Maruyama, Development status of high-efficiency hit solar cells, solar energy materials and solar cells 95 (1) (2011) 18–21, <https://doi.org/10.1016/j.solmat.2010.04.030>, 19th International Photovoltaic Science and Engineering Conference and Exhibition (PVSEC-19) Jeju, Korea, 9–13 November 2009.